

R-matrix electron-impact excitation data for the Mg-like iso-electronic sequence*

L. Fernández-Menchero¹, G. Del Zanna², and N. R. Badnell¹

¹ Department of Physics, University of Strathclyde, Glasgow G4 0NG, UK
e-mail: luis.fernandez-mencher@strath.ac.uk

² Department of Applied Mathematics and Theoretical Physics, University of Cambridge, Cambridge CB3 0WA, UK

Received 22 August 2014 / Accepted 18 September 2014

ABSTRACT

Aims. Emission lines from ions in the Mg-like iso-electronic sequence can be used as reliable diagnostics of temperature and density of astrophysical and fusion plasmas over a wide range of parameters. Data in the literature are quite lacking, there are no calculations for many of the ions in the sequence.

Methods. We have carried-out intermediate coupling frame transformation *R*-matrix calculations which include a total of 283 fine-structure levels in both the configuration interaction target and close-coupling collision expansions. These arise from the configurations $1s^2 2s^2 2p^6 3\{s, p, d\} nl$ with $n = 4, 5$, and for $l = 0-4$.

Results. We obtain ordinary collision strengths and Maxwell-averaged effective collision strengths for the electron-impact excitation of all the ions of the Mg-like sequence, from Al^+ to Zn^{18+} . We compare our results with those from previous *R*-matrix and distorted waves calculations, where available, for some benchmark ions. We find good agreement with the results of previous calculations for the transitions $n = 3-3$. We also find good agreement for the most intense transitions $n = 3-4$. These transitions are important for populating the upper levels of the main diagnostic lines.

Key words. atomic data – techniques: spectroscopic

1. Introduction

Emission lines from magnesium-like ions are observed in a variety of astrophysical sources, such as the solar corona, solar transition region, stars, the interstellar medium, planetary nebulae and novae. They have been used for diagnostics of electron densities, temperatures and chemical abundances of e.g. gaseous nebulae (see, e.g. Si III Nussbaumer 1986 and Rubin et al. 1993) and the solar corona (see, e.g. Si III Dufton et al. 1983; S V Laming et al. 1997; Fe XV Dere et al. 1979). Lines from Si III were also used to suggest that non-Maxwellian electron distributions are present in the solar corona (see, e.g. Dufton et al. 1984 and Keenan et al. 1989).

Despite their importance, there is no *R*-matrix or distorted wave (DW) electron-impact excitation data for many ions in the sequence. Electron-impact excitation data are available for only a few of the most important ions, in most cases being calculated with small basis sets. *R*-matrix calculations for Al^+ have been carried out by Aggarwal & Keenan (1994), with a basis set of 12 close-coupling terms, and Aggarwal (1998) with 20 levels. *R*-matrix calculations for Si^{2+} also exist: Dufton & Kingston (1989), 20 levels, and Griffin et al. (1999), 45 levels with 36 bound ones. Christensen et al. (1986) carried out distorted wave calculations for S^{4+} , Ar^{6+} , Ca^{8+} , Cr^{12+} and Ni^{16+} including 16 levels. Christensen et al. (1986) used the UCL-DW (Eissner 1998) code in conjunction with the JAJOM (Sarah 1972) code.

S^{4+} electron-impact excitation data were also calculated with the *R*-matrix codes by Hudson & Bell (2006) on including 14 terms. Griffin et al. (1999) also carried-out 45 level *R*-matrix calculations for Ar^{6+} and Ti^{10+} .

Fe^{14+} clearly has received special attention, with several distorted wave and *R*-matrix calculations being performed over the years. The most recent are the distorted wave ones from Landi (2011) calculated using the Flexible Atomic Code (FAC) of Gu (2003). Landi (2011) calculated collision data from the lowest 4 levels up to 283 levels of the target. In contrast, the *R*-matrix calculations of Griffin et al. (1999) and Berrington et al. (2005) included just 45 levels in the close-coupling expansion, but determined collision data between all of them. Berrington et al. (2005) made a study of the inclusion of the relativistic effects in the Hamiltonian, comparing the results of Breit-Pauli and Dirac *R*-matrix calculations (DARC). They concluded that the difference was less than the differences which could be expected due to uncertainties in the atomic structure.

Electron-impact excitation data for Ni^{16+} have been calculated by Bhatia & Landi (2011), using the FAC distorted wave code, from the lowest 4 levels up to the 159 levels of their target expansion, and by Hudson et al. (2009, 2012) using the Dirac *R*-matrix suite of codes on including 37 close-coupling levels.

We did not find any atomic collision data in the literature for the rest of the ions in the sequence which we consider here also: P^{3+} , Cl^{5+} , K^{7+} , Sc^{9+} , V^{11+} , Mn^{13+} , Co^{15+} , Cu^{17+} and Zn^{18+} .

In present work we carry-out an intermediate coupling frame transformation (ICFT) *R*-matrix calculation including a total of 283 levels in both the configuration interaction (CI) and the close-coupling expansions. This is the same target basis as used

* These data are made available in the APAP archive via <http://www.apap-network.org>, CHIANTI via <http://www.chiantidatabase.org> and open-ADAS via <http://open.adas.ac.uk>

by Landi (2011), but of course we consider all inelastic transitions. Cascading effects following collisional excitation up to the $n = 5$ shell can be examined within models using this basis set expansion. We use the same basis set and method for the whole iso-electronic sequence, from Al^+ up to Zn^{18+} . The present data therefore includes significantly more transitions than the previous published works for Mg-like ions, where they exist.

Because of its diagnostic importance, the discussion of the target for Si^{2+} deserved special attention. One of the main diagnostic lines turns out to have a strongly-mixed upper level (see below), so we validated our target for this ion with several structure calculations and comparisons with previous calculations and observations. Details are presented in Del Zanna et al. (2014).

The paper is organised as follows. In Sect. 2 we give details of our description of the atomic structure and in Sect. 3 that of the R -matrix calculation. In Sect. 4 we show some representative results and compare them with the results of other R -matrix calculations and with distorted wave ones. The main conclusions are presented in Sect. 5. Atomic units are used unless otherwise specified. The atomic data are made available at our APAP network web page¹. They will also be uploaded online in the CHIANTI atomic database² (Landi et al. 2013) and the Atomic Data and Analysis Structure (open-ADAS³). This work is part of the UK APAP Network and is complementary to our previous work on other sequences. The most recent work was on the boron-like (Liang et al. 2012) and beryllium-like (Fernández-Mencher et al. 2014).

2. Structure

To obtain the wave functions of the isolated target we used the AUTOSTRUCTURE program (Badnell 2011), the approach is the same as that described in our previous work (Fernández-Mencher et al. 2014) but utilizing a different set of configurations. AUTOSTRUCTURE carries-out a diagonalization of the Breit–Pauli Hamiltonian (Eissner et al. 1974) to obtain the eigen states and energies of the target. Relativistic terms, viz. mass-velocity, spin-orbit, and Darwin, are included as a perturbation. We describe the multi-electron electrostatic interactions using a Thomas–Fermi–Dirac–Amaldi model potential with scaling parameters λ_{nl} . We determine the λ_{nl} through a variational method in which we minimize the equally-weighted sum of the energies of all the terms. We included a total of 15 atomic orbitals in the basis set: 1s, 2s, 2p, 3s, 3p, 3d, 4s, 4p, 4d, 4f, 5s, 5p, 5d, 5f, 5g. In the configuration interaction we included all the configurations $\{(1s^2 2s^2 2p^6) 3s^2, 3s 3p, 3s 3d, 3p^2, 3p 3d, 3d^2, 3s nl, 3p nl, 3d nl\}$, for all nl orbitals previously mentioned with $n \geq 4$, for a total of 33 configurations. The minimized values of the scaling parameters are shown in Table 2 for all the ions in the sequence.

For the configuration list detailed above, we obtain 149 LS terms, which on recoupling to take account of the spin-orbit interaction, give rise to 283 levels. The intermediate coupling (IC) energies obtained for the target levels of three sample ions: S^{4+} , Ar^{6+} and Fe^{14+} , are shown in Tables 3–5 respectively. The level energies are compared with the observed ones taken from the tables of the National Institute of Standards and Technology (NIST⁴) database: Martin et al. (1990) for sulphur,

Table 1. Comparison of gf values for some selected transitions of the ion Fe^{14+} . L11: Landi (2011). $A(B)$ denotes $A \times 10^B$.

Transition	gf Present work	gf L11
1–3	3.072 (−3)	3.109 (−3)
1–5	8.154 (−1)	8.118 (−1)
1–26	1.389 (−3)	1.384 (−3)
1–39	1.070 (−1)	1.173 (−1)
1–41	2.917 (−1)	2.858 (−1)
1–47	9.160 (−4)	9.502 (−4)
1–49	5.024 (−3)	5.240 (−3)
1–64	3.400 (−4)	3.538 (−4)
1–73	1.085 (−3)	1.151 (−3)
1–75	3.513 (−3)	3.443 (−3)
1–95	5.105 (−2)	5.588 (−2)
1–97	4.121 (−2)	4.360 (−3)

Saloman (2010) for argon, and Sugar & Corliss (1985) and Shirai et al. (2000) for iron; and with the previous theoretical calculations collected in the CHIANTI database: Christensen et al. (1986) for sulphur and argon, and Landi (2011) for iron. The agreement of the present energies with the observed values is within 1.5%, with a few exceptions in the lower excited singlet levels, and the relative errors are smaller in the present work than in previous theoretical ones with smaller basis sets, and more or less equal to the ones of Landi (2011) with the same configuration set. The energy values for the rest of the levels and the other ions of the sequence not shown in Tables 3–5 can be found online in CHIANTI⁵ and open-ADAS⁶ databases.

To check the quality of the calculated wave functions of the target we compare the oscillator strengths (gf values) for selected transitions in Table 1 for Fe^{14+} with data from Landi (2011), which can be found on line in the CHIANTI database. Very good agreement, within 5%, is found in general.

As a further check of our atomic structure, we show in Fig. 1 a global comparison our oscillator strengths (gf values) with the results of Christensen et al. (1986) for sulphur, and of Landi (2011) for iron. We plot in the x -axis the results of present work, and in the y -axis the comparative ones, so points lying on the diagonal $x = y$ mean complete agreement between the two sets. Practically all the oscillator strengths for transitions (from all lower levels) to the upper $n = 4$ levels lie on the diagonal $x = y$, with deviations smaller than 2% for both ions. For transitions up to $n = 5$ in Fe^{14+} the main body of the points lies on the diagonal also. The points which are spread far from the diagonal (about 100 of the total 1200 shown) correspond to transitions with levels with configurations 5f and 5g, the last orbitals included in our basis. As they are the last bound levels, the description of these excited levels can vary with respect to the previous works since there are no configurations which lie above to “correct” them via CI. This is the likely reason for the differences in the gf values for these transitions. For S^{4+} , the work of Christensen et al. (1986) just shows 22 transitions $k - k'$, with $k = 1-5$ and $k' = 1-16$ levels. The agreement between Christensen et al. (1986) results and ours is better than 5%.

In the particular case of Si^{2+} , the $3s3p\ ^1\text{P}_1 - 3s4s\ ^1\text{S}_0$ transition was used to suggest that non-Maxwellian electron distributions are present in the solar corona (see, e.g. Dufton et al. 1984 and Keenan et al. 1989). It turns out that the upper level $3s4s\ ^1\text{S}_0$ is strongly LS-mixed with the $3p^2\ ^1\text{S}_0$. The energy difference

¹ <http://www.apap-network.org>

² <http://www.chiantidatabase.org>

³ <http://open.adas.ac.uk>

⁴ <http://physics.nist.gov>

⁵ http://www.chiantidatabase.org/chianti_direct_data.html

⁶ <http://open.adas.ac.uk/adf04>

Table 2. Thomas-Fermi-Dirac-Amaldi potential scaling parameters used for the AUTOSTRUCTURE calculations.

Ion	1s 5s	2s 5p	2p 5d	3s 5f	3p 5g	3d	4s	4p	4d	4f
Al ⁺	1.34400	1.07214	1.01666	1.04690	1.06235	1.23400	1.01706	1.01387	1.10681	1.49393
	1.02715	1.02053	1.10823	1.51459	1.81925					
Si ²⁺	1.73313	1.08334	1.01965	1.03490	0.99789	1.03993	1.03517	1.02034	1.06435	1.37638
	1.04415	1.02725	1.07274	1.39217	1.66124					
P ³⁺	1.31200	1.09271	1.02988	1.07910	1.06326	1.14357	1.03794	1.01389	1.03904	1.22747
	1.04221	1.01595	1.03957	1.23875	1.44231					
S ⁴⁺	1.31500	1.10247	1.03513	1.09136	1.06747	1.13039	1.04713	1.01749	1.03408	1.18375
	1.05080	1.01965	1.03441	1.19243	1.36751					
Cl ⁵⁺	1.31800	1.11222	1.03990	1.10240	1.07190	1.12426	1.05636	1.02187	1.03354	1.15522
	1.05946	1.02299	1.03376	1.16377	1.31977					
Ar ⁶⁺	1.34700	1.12220	1.04434	1.11263	1.07629	1.12148	1.06523	1.02571	1.03500	1.13883
	1.06641	1.02736	1.03519	1.14608	1.28770					
K ⁷⁺	1.36000	1.13260	1.04869	1.12258	1.08058	1.12038	1.07404	1.03031	1.03691	1.12819
	1.07563	1.03159	1.03704	1.13482	1.26768					
Ca ⁸⁺	1.38000	1.14363	1.05300	1.13246	1.08475	1.12040	1.08293	1.03469	1.04519	1.12099
	1.08447	1.03586	1.03934	1.11783	1.26846					
Sc ⁹⁺	1.42000	1.15542	1.05735	1.14249	1.08663	1.12273	1.09219	1.03331	1.03320	1.11733
	1.09237	1.03959	1.04200	1.12132	1.24628					
Ti ¹⁰⁺	1.46000	1.16802	1.06185	1.15263	1.09347	1.12186	1.10181	1.04378	1.04422	1.12046
	1.10209	1.04275	1.04311	1.11802	1.23817					
V ¹¹⁺	1.50000	1.18186	1.06655	1.16352	1.09783	1.12302	1.11220	1.04871	1.04620	1.11340
	1.11232	1.04786	1.04680	1.11587	1.23860					
Cr ¹²⁺	1.56000	1.19689	1.07149	1.17488	1.10258	1.12427	1.12322	1.05386	1.04925	1.10821
	1.12252	1.05168	1.04961	1.11491	1.24449					
Mn ¹³⁺	1.64000	1.21343	1.07674	1.18678	1.10719	1.12572	1.13501	1.05922	1.05155	1.10751
	1.13374	1.05684	1.05213	1.11477	1.24541					
Fe ¹⁴⁺	1.69000	1.23152	1.08238	1.19961	1.11209	1.12721	1.14749	1.06516	1.05393	1.10738
	1.14555	1.06200	1.05476	1.11545	1.24581					
Co ¹⁵⁺	1.79000	1.25159	1.08844	1.21358	1.11086	1.12876	1.16147	1.06968	1.05656	1.10865
	1.15886	1.14061	1.05743	1.11612	1.24721					
Ni ¹⁶⁺	1.93000	1.27454	1.09554	1.23480	1.10581	1.13033	1.17661	1.07383	1.05870	1.10693
	1.17289	1.07547	1.06081	1.11720	1.25000					
Cu ¹⁷⁺	2.10000	1.29772	1.10194	1.24413	1.12574	1.13223	1.19193	1.08030	1.06160	1.10980
	1.18771	1.08167	1.06291	1.11855	1.25459					
Zn ¹⁸⁺	2.34000	1.32453	1.10947	1.26090	1.13134	1.13389	1.20880	1.08669	1.06429	1.11068
	1.20360	1.08738	1.06568	1.11906	1.25724					

between these two levels is only 5625 cm⁻¹. During the optimization process of the scaling parameters of this ion we had to be careful to get the correct mixing between these two levels. The *A*-values for the decays from these levels are very sensitive to the structure. The scaling parameters which lead to the optimum value of the Einstein coefficient for that transition are the ones shown in Table 2. We refer to Del Zanna et al. (2014) for a more detailed description of this specific ion, comparisons with previous calculations and with observations.

3. Scattering

For the scattering calculation, we used the same approach as in our previous work (Fernández-Menchero et al. 2014), which consists of an *R*-matrix formalism (Hummer et al. 1993; Berrington et al. 1995) combined with an intermediate coupling frame transformation (Badnell & Griffin 2001; Badnell et al. 2001) to include the spin-orbit mixing efficiently and accurately.

The calculation in the inner region of the *R*-matrix method was split into two parts, one including electron exchange effects and a second one using a non-exchange approximation.

The exchange calculation included angular momenta up to $2J = 30$, and the non exchange extended up to $2J = 80$.

For higher angular momenta up to infinity, we used the top-up formula of the Burgess sum rule (Burgess 1974) for dipole allowed transitions, and a geometric series for the remaining non-forbidden transitions, i.e. those with a non-zero infinite energy Born limit (Badnell & Griffin 2001).

The *R*-matrix outer region calculation was also split into two parts. For the resonance region, where impact energies are below the excitation energy of the last calculated level, a fine energy mesh was applied in order to resolve the resonances. For energies above the last energy threshold a coarse mesh was used to resolve the smooth background. This coarse mesh was around $10^{-4}z^2$ Ry, with z the ion charge $Z - 12$, Z being the atomic number.

In the resonance region, we have the difficulty that the characteristic scattering energy increases as a factor z^2 with the charge of the ion, nevertheless the width of the resonances remains constant. If we attempt to resolve the resonances to the same degree along the whole sequence we have then to reduce the energy step of the fine mesh by a factor z^2 too. This number of points becomes computationally unreasonable for the highest few charge states in the sequence. We used the same practical criterion as in Witthoeft et al. (2007) and we increased the number of grid points by a factor z ; this samples and converges the resonance structure satisfactorily. Thus, we use a fine energy

Table 3. S⁴⁺ target levels.

<i>i</i>	Conf. Level	E_{th}	(%)	E_{NIST}	E_{C86}	(%)	<i>i</i>	Conf. Level	E_{th}	(%)	E_{NIST}	E_{C86} (%)
1	3s ² ¹ S ₀	0.	(0.0)	0.	0.	(0.0)	50	3s 5p ¹ P ₁ ^o	446 297.	(0.4)	447 926.	– (–)
2	3s 3p ³ P ₀ ^o	81 903.	(1.4)	83 024.	81 315.	(2.1)	51	3p 4p ¹ P ₁	447 561.	(–)	–	– (–)
3	3s 3p ³ P ₁ ^o	82 281.	(1.3)	83 394.	81 667.	(2.1)	52	3p 4p ³ D ₁	449 900.	(–)	–	– (–)
4	3s 3p ³ P ₂ ^o	83 055.	(1.3)	84 155.	82 380.	(2.1)	53	3p 4p ³ D ₂	450 254.	(–)	–	– (–)
5	3s 3p ¹ P ₁ ^o	129 469.	(1.8)	127 151.	128 491.	(1.1)	54	3p 4p ³ D ₃	450 935.	(–)	–	– (–)
6	3p ² ¹ D ₂	192 961.	(0.4)	193 739.	191 788.	(1.0)	55	3p 4p ³ P ₀	455 933.	(–)	–	– (–)
7	3p ² ³ P ₀	200 144.	(0.1)	199 967.	198 954.	(0.5)	56	3p 4p ³ P ₁	456 148.	(–)	–	– (–)
8	3p ² ³ P ₁	200 551.	(0.1)	200 371.	204 550.	(2.1)	57	3p 4p ³ P ₂	456 646.	(–)	–	– (–)
9	3p ² ³ P ₂	201 338.	(0.1)	201 146.	200 051.	(0.5)	58	3p 4p ³ S ₁	457 873.	(–)	–	– (–)
10	3s 3d ³ D ₁	236 311.	(0.6)	234 942.	234 377.	(0.2)	59	3p 4p ¹ D ₂	458 379.	(–)	–	– (–)
11	3s 3d ³ D ₂	236 338.	(0.6)	234 947.	234 399.	(0.2)	60	3s 5d ³ D ₁	465 445.	(0.6)	468 048.	– (–)
12	3s 3d ³ D ₃	236 379.	(0.6)	234 956.	234 432.	(0.2)	61	3s 5d ³ D ₂	465 479.	(0.6)	468 077.	– (–)
13	3p ² ¹ S ₀	238 460.	(1.3)	235 350.	237 230.	(0.8)	62	3s 5d ³ D ₃	465 534.	(0.6)	468 132.	– (–)
14	3s 3d ¹ D ₂	276 501.	(2.1)	270 700.	272 851.	(0.8)	63	3s 5d ¹ D ₂	468 746.	(0.3)	470 229.	– (–)
15	3s 4s ³ S ₁	308 970.	(0.8)	311 595.	309 328.	(0.7)	64	3s 5f ³ F ₂ ^o	471 107.	(0.6)	473 926.	– (–)
16	3s 4s ¹ S ₀	318 555.	(0.5)	320 108.	319 632.	(0.1)	65	3s 5f ³ F ₃ ^o	471 109.	(0.6)	473 926.	– (–)
17	3p 3d ³ F ₂ ^o	323 259.	(0.0)	323 133.	–	(–)	66	3s 5f ³ F ₄ ^o	471 112.	(0.6)	473 930.	– (–)
18	3p 3d ³ F ₃ ^o	323 692.	(0.0)	323 547.	–	(–)	67	3s 5g ¹ G ₄	471 314.	(0.7)	474 477.	– (–)
19	3p 3d ³ F ₄ ^o	324 247.	(0.1)	324 080.	–	(–)	68	3s 5g ³ G ₃	471 344.	(0.7)	474 507.	– (–)
20	3p 3d ¹ D ₀ ^o	328 664.	(0.1)	328 454.	–	(–)	69	3s 5g ³ G ₄	471 356.	(0.7)	474 516.	– (–)
21	3s 4p ³ P ₀ ^o	346 443.	(0.8)	349 122.	–	(–)	70	3s 5g ³ G ₅	471 365.	(0.7)	474 522.	– (–)
22	3s 4p ³ P ₁ ^o	346 444.	(0.8)	349 161.	–	(–)	71	3s 5f ¹ F ₃ ^o	473 887.	(0.4)	475 802.	– (–)
23	3s 4p ³ P ₂ ^o	346 462.	(0.9)	349 478.	–	(–)	72	3p 4p ¹ S ₀	474 364.	(–)	–	– (–)
24	3s 4p ¹ P ₁ ^o	347 131.	(0.7)	349 534.	–	(–)	73	3d ² ³ F ₂	475 884.	(–)	–	– (–)
25	3p 3d ³ P ₂ ^o	347 670.	(0.7)	345 338.	–	(–)	74	3d ² ³ F ₃	475 930.	(–)	–	– (–)
26	3p 3d ³ P ₀ ^o	347 800.	(0.6)	345 713.	–	(–)	75	3d ² ³ F ₄	475 990.	(–)	–	– (–)
27	3p 3d ³ P ₁ ^o	347 949.	(0.6)	345 953.	–	(–)	76	3d ² ¹ G ₄	480 402.	(–)	–	– (–)
28	3p 3d ³ D ₁ ^o	349 518.	(0.5)	347 841.	–	(–)	77	3d ² ¹ D ₂	488 959.	(–)	–	– (–)
29	3p 3d ³ D ₂ ^o	349 696.	(0.5)	348 010.	–	(–)	78	3d ² ³ P ₀	491 818.	(–)	–	– (–)
30	3p 3d ³ D ₃ ^o	349 842.	(0.5)	348 132.	–	(–)	79	3d ² ³ P ₁	491 836.	(–)	–	– (–)
31	3p 3d ¹ F ₃ ^o	371 531.	(1.3)	366 862.	–	(–)	80	3d ² ³ P ₂	491 871.	(–)	–	– (–)
32	3p 3d ¹ P ₁ ^o	386 552.	(–)	–	(–)	81	3p 4d ¹ D ₂ ^o	498 179.	(–)	–	– (–)	
33	3s 4d ³ D ₁	393 859.	(0.5)	396 026.	–	(–)	82	3p 4d ³ D ₀ ^o	498 944.	(–)	–	– (–)
34	3s 4d ³ D ₂	393 880.	(0.5)	396 040.	–	(–)	83	3p 4d ³ D ₂ ^o	499 039.	(–)	–	– (–)
35	3s 4d ³ D ₃	393 910.	(0.5)	396 061.	–	(–)	84	3p 4d ³ D ₃ ^o	499 215.	(–)	–	– (–)
36	3s 4d ¹ D ₂	395 943.	(0.4)	397 605.	–	(–)	85	3p 4d ³ F ₂ ^o	500 705.	(–)	–	– (–)
37	3s 4f ³ F ₂ ^o	408 383.	(0.6)	410 910.	–	(–)	86	3p 4d ³ F ₃ ^o	501 011.	(–)	–	– (–)
38	3s 4f ³ F ₃ ^o	408 390.	(0.6)	410 912.	–	(–)	87	3p 4d ³ F ₄ ^o	501 490.	(–)	–	– (–)
39	3s 4f ³ F ₄ ^o	408 400.	(0.6)	410 918.	–	(–)	88	3p 4d ¹ F ₃ ^o	504 591.	(–)	–	– (–)
40	3p 4s ³ P ₀ ^o	418 505.	(0.5)	420 742.	–	(–)	89	3p 4d ³ P ₂ ^o	505 416.	(–)	–	– (–)
41	3p 4s ³ P ₁ ^o	418 830.	(0.5)	421 057.	–	(–)	90	3p 4d ³ P ₀ ^o	505 731.	(–)	–	– (–)
42	3s 4f ¹ F ₃ ^o	418 865.	(0.2)	417 985.	–	(–)	91	3p 4d ³ P ₀ ^o	505 910.	(–)	–	– (–)
43	3p 4s ³ P ₂ ^o	419 633.	(0.5)	421 943.	–	(–)	92	3p 4d ¹ P ₁ ^o	510 422.	(–)	–	– (–)
44	3p 4s ¹ P ₁ ^o	423 569.	(0.2)	424 526.	–	(–)	93	3p 4f ¹ F ₃	510 643.	(–)	–	– (–)
45	3s 5s ³ S ₁	425 829.	(0.6)	428 439.	–	(–)	94	3p 4f ³ G ₃	513 878.	(–)	–	– (–)
46	3s 5s ¹ S ₀	428 426.	(0.6)	430 802.	–	(–)	95	3p 4f ³ G ₄	514 138.	(–)	–	– (–)
47	3s 5p ³ P ₀	442 570.	(0.6)	445 304.	–	(–)	96	3p 4f ³ F ₂	514 457.	(–)	–	– (–)
48	3s 5p ³ P ₁	442 616.	(0.6)	445 350.	–	(–)	97	3p 4f ³ F ₃	514 706.	(–)	–	– (–)
49	3s 5p ³ P ₂	442 711.	(0.6)	445 498.	–	(–)	98	3p 4f ³ G ₅	514 838.	(–)	–	– (–)

Notes. Key: *i*: level index; Conf.: configuration; Level: level IC designation; E_{th} : theoretical level energy (this work); E_{NIST} : observed energy from the NIST database (Martin et al. 1995); E_{C86} : previous theoretical calculation (Christensen et al. 1986); %: percentage difference between theoretical and NIST data. All energies are in cm⁻¹.

mesh step which varies continuously versus the ionic charge, from 1.4×10^{-4} for Al⁺ up to 3.6×10^{-6} for Zn¹⁸⁺.

We obtain the Maxwell-averaged effective collision strengths for electron-impact excitation, $\Upsilon(i-j)$, on performing a convolution of the ordinary collision strengths, Ω , with a Maxwellian velocity distribution for the electrons:

$$\Upsilon(i-j) = \int_0^{\infty} du \exp(-u) \Omega(i-j), \quad (1)$$

where $u = E/kT$, E is the final energy of the scattered electron, T the electron temperature and k the Boltzmann constant. We calculated the effective collision strengths for a wide range of temperatures, from $\sim z^2 \times 10^2$ to $\sim z^2 \times 10^5$ K, which covers the temperature range of interest for each ion for both astrophysical and fusion plasmas.

Nevertheless, in some radiating astrophysical sources the electron velocity distribution differs from a Maxwellian one, e.g. the solar wind (Bryant 1996). As such, the study of non-Maxwellian velocity distributions has become more intensive in

Table 4. Ar⁶⁺ target levels.

<i>i</i>	Conf. Level	E_{th}	(%)	E_{NIST}	E_{C86}	(%)	<i>i</i>	Conf. Level	E_{th}	(%)	E_{NIST}	E_{C86} (%)
1	3s ² ¹ S ₀	0.	(0.0)	0.	0.	(0.0)	50	3d ² ³ P ₀	675 794.	(1.0)	669 285.	– (–)
2	3s 3p ³ P ₀ ₁	112 070.	(0.9)	113 101.	112 206.	(0.8)	51	3d ² ³ P ₁	675 844.	(1.0)	669 366.	– (–)
3	3s 3p ³ P ₁ ₂	112 889.	(0.9)	113 906.	112 854.	(0.9)	52	3d ² ³ P ₂	675 949.	(1.0)	669 410.	– (–)
4	3s 3p ³ P ₂ ₁	114 593.	(0.9)	115 590.	114 028.	(1.4)	53	3p 4p ¹ P ₁	699 723.	(0.2)	698 350.	– (–)
5	3s 3p ¹ P ₁ ₀	173 751.	(1.8)	170 722.	172 792.	(1.2)	54	3p 4p ³ D ₁	704 134.	(0.3)	701 808.	– (–)
6	3p ² ¹ D ₂	264 530.	(0.1)	264 749.	263 545.	(0.5)	55	3p 4p ³ D ₂	704 928.	(0.3)	702 553.	– (–)
7	3p ² ³ P ₀	270 704.	(0.3)	269 836.	270 316.	(0.2)	56	3p 4p ³ D ₃	706 558.	(–)	–	– (–)
8	3p ² ³ P ₁	271 641.	(0.3)	270 777.	270 579.	(0.1)	57	3p 4p ³ S ₁	709 276.	(0.2)	708 189.	– (–)
9	3p ² ³ P ₂	273 432.	(0.3)	272 562.	272 335.	(0.1)	58	3p 4p ³ P ₀	710 505.	(–)	–	– (–)
10	3p ² ¹ S ₀	320 974.	(1.3)	316 717.	324 713.	(2.5)	59	3p 4p ³ P ₁	711 664.	(0.0)	711 890.	– (–)
11	3s 3d ³ D ₁	326 054.	(0.6)	324 104.	324 833.	(0.2)	60	3d ² ¹ S ₀	712 070.	(0.6)	707 626.	– (–)
12	3s 3d ³ D ₂	326 141.	(0.6)	324 141.	319 753.	(1.4)	61	3p 4p ³ P ₂	712 647.	(–)	–	– (–)
13	3s 3d ³ D ₃	326 273.	(0.6)	324 205.	324 702.	(0.2)	62	3s 5s ³ S ₁	717 638.	(0.3)	715 747.	– (–)
14	3s 3d ¹ D ₂	377 167.	(1.9)	370 294.	374 303.	(1.1)	63	3s 5s ¹ S ₀	717 997.	(0.4)	714 794.	– (–)
15	3p 3d ³ F ₂ ₀	444 677.	(0.3)	443 362.	–	(–)	64	3p 4p ¹ D ₂	721 692.	(0.2)	720 475.	– (–)
16	3p 3d ³ F ₃ ₀	445 701.	(0.2)	444 780.	–	(–)	65	3s 5p ³ P ₀ ₀	737 406.	(0.3)	739 463.	– (–)
17	3p 3d ³ F ₄ ₀	446 969.	(0.2)	446 011.	–	(–)	66	3s 5p ³ P ₁ ₀	737 500.	(0.3)	739 690.	– (–)
18	3p 3d ¹ D ₂ ₀	451 352.	(0.2)	450 477.	–	(–)	67	3s 5p ³ P ₂ ₀	737 727.	(0.3)	739 763.	– (–)
19	3p 3d ³ P ₂ ₀	475 022.	(0.6)	472 282.	–	(–)	68	3s 5p ¹ P ₁	739 534.	(0.3)	741 843.	– (–)
20	3p 3d ³ P ₀ ₁	475 699.	(0.6)	472 875.	–	(–)	69	3p 4p ¹ S ₀	745 566.	(–)	–	– (–)
21	3p 3d ³ P ₀ ₀	476 301.	(0.5)	473 810.	–	(–)	70	3s 5d ³ D ₁	769 630.	(0.4)	772 345.	– (–)
22	3p 3d ³ D ₁ ₀	477 901.	(0.6)	475 217.	–	(–)	71	3s 5d ³ D ₂	769 646.	(0.3)	772 349.	– (–)
23	3p 3d ³ D ₂ ₀	478 313.	(0.6)	475 585.	–	(–)	72	3s 5d ³ D ₃	769 671.	(0.3)	772 352.	– (–)
24	3p 3d ³ D ₃ ₀	478 560.	(0.6)	475 762.	–	(–)	73	3s 5d ¹ D ₂	770 662.	(0.3)	772 930.	– (–)
25	3s 4s ³ S ₁	511 372.	(0.5)	514 076.	512 309.	(0.3)	74	3p 4d ¹ D ₂ ₀	771 823.	(–)	–	– (–)
26	3p 3d ¹ F ₀ ₁	515 169.	(1.0)	510 268.	–	(–)	75	3p 4d ³ D ₀ ₂	772 078.	(–)	–	– (–)
27	3s 4s ¹ S ₀	523 618.	(1.0)	528 910.	525 323.	(0.7)	76	3p 4d ³ D ₀ ₂	772 376.	(–)	–	– (–)
28	3p 3d ¹ P ₀ ₁	524 282.	(1.4)	517 105.	–	(–)	77	3p 4d ³ D ₀ ₃	772 643.	(–)	–	– (–)
29	3s 4p ³ P ₀ ₀	565 087.	(0.2)	563 880.	–	(–)	78	3p 4d ³ F ₂ ₀	775 767.	(–)	–	– (–)
30	3s 4p ³ P ₀ ₁	565 295.	(0.2)	564 418.	–	(–)	79	3p 4d ³ F ₃ ₀	776 096.	(–)	–	– (–)
31	3s 4p ³ P ₀ ₂	565 840.	(0.2)	564 728.	–	(–)	80	3p 4d ³ F ₄ ₀	777 319.	(–)	–	– (–)
32	3s 4p ¹ P ₁ ₀	568 205.	(0.3)	569 797.	–	(–)	81	3p 4d ¹ F ₃ ₀	777 743.	(–)	–	– (–)
33	3s 4d ³ D ₁	632 497.	(0.3)	634 605.	–	(–)	82	3s 5g ³ G ₃	778 817.	(–)	–	– (–)
34	3s 4d ³ D ₂	632 562.	(0.3)	634 639.	–	(–)	83	3s 5g ³ G ₄	778 990.	(–)	–	– (–)
35	3s 4d ³ D ₃	632 659.	(0.3)	634 701.	–	(–)	84	3s 5g ³ G ₅	779 227.	(–)	–	– (–)
36	3s 4d ¹ D ₂	633 443.	(0.3)	635 295.	–	(–)	85	3s 5g ¹ G ₄	780 270.	(–)	–	– (–)
37	3d ² ³ F ₂	656 922.	(0.5)	653 904.	–	(–)	86	3s 5f ³ F ₂ ₀	781 571.	(–)	–	– (–)
38	3d ² ³ F ₃	657 058.	(0.5)	654 038.	–	(–)	87	3s 5f ³ F ₃ ₀	781 629.	(–)	–	– (–)
39	3p 4s ³ P ₀ ₀	657 189.	(–)	–	–	(–)	88	3s 5f ³ F ₄ ₀	781 714.	(0.3)	784 394.	– (–)
40	3d ² ³ F ₄	657 237.	(0.5)	654 126.	–	(–)	89	3p 4d ³ P ₂ ₀	782 742.	(–)	–	– (–)
41	3s 4f ³ F ₀ ₁	657 616.	(0.4)	660 075.	–	(–)	90	3p 4d ³ P ₁ ₀	783 337.	(–)	–	– (–)
42	3s 4f ³ F ₀ ₂	657 632.	(0.4)	660 112.	–	(–)	91	3p 4d ³ P ₀ ₀	783 742.	(–)	–	– (–)
43	3s 4f ³ F ₄ ₀	657 653.	(0.4)	660 122.	–	(–)	92	3s 5f ¹ F ₃ ₀	785 912.	(–)	–	– (–)
44	3p 4s ³ P ₀ ₁	657 877.	(–)	–	–	(–)	93	3p 4d ¹ P ₁ ₀	787 802.	(–)	–	– (–)
45	3p 4s ³ P ₀ ₂	659 674.	(–)	–	–	(–)	94	3p 4f ¹ F ₃ ₀	793 794.	(–)	–	– (–)
46	3s 4f ¹ F ₃ ₀	666 689.	(0.1)	667 496.	–	(–)	95	3p 4f ³ F ₂ ₀	797 319.	(–)	–	– (–)
47	3p 4s ¹ P ₁ ₀	666 982.	(–)	–	–	(–)	96	3p 4f ³ F ₃ ₀	797 484.	(–)	–	– (–)
48	3d ² ¹ G ₄	670 605.	(0.4)	668 061.	–	(–)	97	3p 4f ³ F ₄ ₀	797 828.	(–)	–	– (–)
49	3d ² ¹ D ₂	673 323.	(1.0)	666 550.	–	(–)	98	3p 4f ³ G ₃ ₀	801 999.	(–)	–	– (–)

Notes. Key: *i*: level index; Conf.: configuration; Level: level IC designation; E_{th} : theoretical level energy (this work); E_{NIST} : observed energy from the NIST database (Saloman 2010); E_{C86} : previous theoretical calculation (Christensen et al. 1986); %: percentage difference between theoretical and NIST data. All energies are in cm⁻¹.

recent years, see for example Dudík et al. (2014a,b); Storey & Sochi (2013); Dzifčáková & Dudík (2013). In models with enhanced high-energy tails, the kinetic energy of the electrons typically follows a κ distribution:

$$f(E; \kappa, E_{\kappa}) = \frac{\Gamma(\kappa + 1)}{\Gamma(\kappa - \frac{1}{2})} \frac{2}{\sqrt{\pi}} \frac{1}{\kappa E_{\kappa}} \left(\frac{E}{\kappa E_{\kappa}} \right)^{1/2} \left(1 + \frac{E}{\kappa E_{\kappa}} \right)^{-(\kappa+1)}, \quad (2)$$

where κ parameterizes the family, E_{κ} is the characteristic energy such that $\kappa E_{\kappa}/(\kappa - 3/2) = kT_{\text{eff}}$, where T_{eff} is the effective

temperature, i.e. $kT_{\text{eff}} = 2\bar{E}/3$, \bar{E} being the mean electron energy. The κ distribution tends to a Maxwellian one as κ tends to infinity.

In the Maxwellian case, the effective collision strengths for de-excitation, $\mathcal{J}(i - j)$, are equal to the ones for excitation. In the case of a non-Maxwellian distribution this is no longer true. The de-excitation effective collision strength is given by (1), but with the Maxwellian distribution replaced by the kappa one (2). The excitation effective collision strength expression involves

Table 5. Fe¹⁴⁺ target levels.

<i>i</i>	Conf.	Level	E_{th}	(%)	E_{NIST}	E_{L11}	(%)	<i>i</i>	Conf.	Level	E_{th}	(%)	E_{NIST}	E_{L11}	(%)
1	3s ²	¹ S ₀	0.	(0.0)	0.	0.	(0.0)	50	3s 4f	³ F ₂ ⁰	2 106 878.	(0.1)	2 108 520.	2 107 229.	(0.1)
2	3s 3p	³ P ₀ ⁰	233 066.	(0.3)	233 842.	233 068.	(0.3)	51	3s 4f	³ F ₃ ⁰	2 107 113.	(0.1)	2 108 620.	2 107 424.	(0.1)
3	3s 3p	³ P ₁ ¹	238 974.	(0.3)	239 660.	238 900.	(0.3)	52	3s 4f	³ F ₄ ¹	2 107 428.	(0.1)	2 108 880.	2 107 701.	(0.1)
4	3s 3p	³ P ₂ ⁰	253 015.	(0.3)	253 820.	252 918.	(0.4)	53	3s 4f	¹ F ₃ ⁰	2 123 577.	(0.0)	2 123 150.	2 124 055.	(0.0)
5	3s 3p	¹ P ₁ ¹	356 807.	(1.4)	351 911.	356 127.	(1.2)	54	3p 4p	¹ P ₁	2 153 900.	(–)	–	2 167 344.	(–)
6	3p ²	³ P ₀	557 614.	(0.6)	554 524.	556 995.	(0.4)	55	3p 4p	³ D ₁	2 167 755.	(–)	–	2 153 046.	(–)
7	3p ²	¹ D ₂	561 312.	(0.3)	559 600.	560 266.	(0.1)	56	3p 4p	³ D ₂	2 169 704.	(–)	–	2 169 174.	(–)
8	3p ²	³ P ₁	567 380.	(0.5)	564 602.	566 833.	(0.4)	57	3p 4p	³ P ₀	2 175 168.	(–)	–	2 175 103.	(–)
9	3p ²	³ P ₂	584 191.	(0.4)	581 803.	583 564.	(0.3)	58	3p 4p	³ P ₁	2 182 627.	(–)	–	2 182 791.	(–)
10	3p ²	¹ S ₀	666 738.	(1.1)	659 627.	665 768.	(0.9)	59	3p 4p	³ D ₃	2 184 291.	(–)	–	2 184 243.	(–)
11	3s 3d	³ D ₁	682 739.	(0.6)	678 772.	680 146.	(0.2)	60	3p 4p	³ P ₂	2 190 338.	(–)	–	2 190 674.	(–)
12	3s 3d	³ D ₂	684 031.	(0.6)	679 785.	681 129.	(0.2)	61	3p 4p	³ S ₁	2 192 694.	(–)	–	2 192 598.	(–)
13	3s 3d	³ D ₃	686 015.	(0.7)	681 416.	682 667.	(0.2)	62	3p 4p	¹ D ₂	2 208 825.	(–)	–	2 209 221.	(–)
14	3s 3d	¹ D ₂	772 235.	(1.3)	762 093.	769 370.	(1.0)	63	3p 4p	¹ S ₀	2 238 710.	(–)	–	2 239 314.	(–)
15	3p 3d	³ F ₂ ⁰	932 223.	(0.4)	928 241.	928 787.	(0.1)	64	3p 4d	³ D ₁ ⁰	2 313 442.	(–)	–	2 312 000.	(–)
16	3p 3d	³ F ₃ ⁰	942 210.	(0.4)	938 126.	938 555.	(0.0)	65	3p 4d	¹ D ₂ ⁰	2 313 752.	(–)	–	2 312 327.	(–)
17	3p 3d	¹ D ₂ ⁰	952 970.	(0.5)	948 513.	949 447.	(0.1)	66	3p 4d	³ D ₂ ⁰	2 314 325.	(–)	–	2 312 836.	(–)
18	3p 3d	³ F ₄ ⁰	953 701.	(0.4)	949 658.	949 928.	(0.0)	67	3p 4d	³ D ₃ ⁰	2 316 070.	(–)	–	2 314 466.	(–)
19	3p 3d	³ D ₁ ⁰	989 033.	(0.6)	982 868.	986 083.	(0.3)	68	3p 4d	³ F ₂ ⁰	2 330 664.	(–)	–	2 329 648.	(–)
20	3p 3d	³ P ₂ ⁰	989 882.	(0.6)	983 514.	986 408.	(0.3)	69	3p 4d	³ F ₃ ⁰	2 332 177.	(–)	–	2 331 021.	(–)
21	3p 3d	³ D ₃ ⁰	1 001 475.	(0.7)	994 852.	997 944.	(0.3)	70	3p 4d	³ F ₄ ⁰	2 339 130.	(–)	–	2 338 064.	(–)
22	3p 3d	³ P ₀ ⁰	1 001 577.	(0.6)	995 889.	998 763.	(0.3)	71	3p 4d	¹ F ₃ ⁰	2 339 805.	(–)	–	2 338 703.	(–)
23	3p 3d	³ P ₁ ⁰	1 002 173.	(0.6)	996 243.	999 173.	(0.3)	72	3p 4d	³ P ₂ ⁰	2 343 664.	(–)	–	2 342 598.	(–)
24	3p 3d	³ D ₂ ⁰	1 002 870.	(0.6)	996 623.	999 579.	(0.3)	73	3p 4d	³ P ₁ ⁰	2 344 816.	(–)	–	2 344 3851.	(–)
25	3p 3d	¹ F ₃ ⁰	1 073 940.	(1.1)	1 062 515.	1 070 795.	(0.8)	74	3p 4d	³ P ₀ ⁰	2 348 606.	(–)	–	2 347 824.	(–)
26	3p 3d	¹ P ₁ ⁰	1 086 964.	(1.1)	1 074 887.	1 083 826.	(0.8)	75	3p 4d	¹ P ₀ ⁰	2 352 772.	(–)	–	2 351 662.	(–)
27	3d ²	³ F ₂	1 378 012.	(0.6)	1 370 331.	1 372 401.	(0.2)	76	3p 4f	³ G ₃	2 379 548.	(0.0)	2 380 160.	2 379 431.	(0.0)
28	3d ²	³ F ₃	1 380 088.	(0.6)	1 372 035.	1 373 989.	(0.1)	77	3p 4f	¹ F ₃	2 386 313.	(0.0)	2 386 700.	2 386 431.	(0.0)
29	3d ²	³ F ₄	1 382 658.	(0.6)	1 374 056.	1 375 938.	(0.1)	78	3p 4f	³ G ₄	2 386 591.	(0.0)	2 386 700.	2 386 689.	(0.0)
30	3d ²	¹ D ₂	1 413 181.	(0.8)	1 402 592.	1 407 428.	(0.3)	79	3p 4f	³ F ₂	2 390 046.	(0.0)	2 390 100.	2 390 113.	(0.0)
31	3d ²	³ P ₀	1 415 071.	(–)	–	1 409 508.	(–)	80	3p 4f	³ F ₃	2 399 289.	(0.1)	2 402 100.	2 399 797.	(0.1)
32	3d ²	³ P ₁	1 415 858.	(–)	–	1 410 109.	(–)	81	3p 4f	³ G ₅	2 401 445.	(0.0)	2 402 100.	2 401 746.	(0.0)
33	3d ²	³ P ₂	1 418 098.	(0.7)	1 407 773.	1 411 644.	(0.3)	82	3p 4f	³ F ₄	2 402 058.	(–)	–	2 402 508.	(–)
34	3d ²	¹ G ₄	1 418 376.	(0.8)	1 407 058.	1 412 127.	(0.4)	83	3p 4f	³ D ₃	2 413 767.	(0.0)	2 413 000.	2 414 121.	(0.0)
35	3d ²	¹ S ₀	1 503 783.	(1.1)	1 487 054.	1 498 669.	(0.8)	84	3p 4f	³ D ₂	2 416 798.	(0.1)	2 414 300.	2 417 276.	(0.1)
36	3s 4s	³ S ₁	1 761 406.	(0.1)	1 763 700.	1 760 911.	(0.2)	85	3p 4f	³ D ₁	2 419 888.	(0.0)	2 420 100.	2 420 513.	(0.0)
37	3s 4s	¹ S ₀	1 785 747.	(0.1)	1 787 000.	1 786 053.	(0.1)	86	3p 4f	¹ G ₄	243 2262.	(0.1)	2 428 700.	2 432 909.	(0.2)
38	3s 4p	³ P ₀ ⁰	1 880 397.	(–)	–	1 880 319.	(–)	87	3p 4f	¹ D ₂	2 438 337.	(0.1)	2 436 000.	2 438 982.	(0.1)
39	3s 4p	³ P ₁ ⁰	1 880 925.	(–)	–	1 880 746.	(–)	88	3d 4s	³ D ₁	2 461 314.	(–)	–	2 458 815.	(–)
40	3s 4p	³ P ₂ ⁰	1 887 467.	(–)	–	1 887 756.	(–)	89	3d 4s	³ D ₂	2 462 341.	(–)	–	2 459 676.	(–)
41	3s 4p	¹ P ₀ ⁰	1 888 045.	(0.1)	1 889 970.	1 888 125.	(0.1)	90	3d 4s	³ D ₃	2 464 548.	(–)	–	2 461 461.	(–)
42	3s 4d	³ D ₁	2 030 669.	(0.0)	2 031 310.	2 029 564.	(0.1)	91	3d 4s	¹ D ₂	2 473 294.	(–)	–	2 470 364.	(–)
43	3s 4d	³ D ₂	2 031 472.	(0.0)	2 032 020.	2 030 329.	(0.1)	92	3s 5s	³ S ₁	2 508 057.	(1.4)	2 544 800.	2 507 572.	(1.5)
44	3s 4d	³ D ₃	2 032 758.	(0.0)	2 033 180.	2 031 544.	(0.1)	93	3s 5s	¹ S ₀	2 517 260.	(–)	–	2 517 043.	(–)
45	3s 4d	¹ D ₂	2 034 320.	(0.0)	2 035 280.	2 033 212.	(0.1)	94	3d 4p	¹ D ₂ ⁰	2 564 016.	(–)	–	2 561 170.	(–)
46	3p 4s	³ P ₀ ⁰	2 052 338.	(–)	–	2 051 779.	(–)	95	3s 5p	³ P ₁ ⁰	2 564 893.	(–)	–	2 564 254.	(–)
47	3p 4s	³ P ₁ ⁰	2 056 014.	(–)	–	2 055 514.	(–)	96	3s 5p	³ P ₀ ⁰	2 565 001.	(–)	–	2 564 597.	(–)
48	3p 4s	³ P ₂ ⁰	2 072 095.	(–)	–	2 072 084.	(–)	97	3s 5p	¹ P ₁	2 567 298.	(0.0)	2 567 000.	2 566 041.	(0.0)
49	3p 4s	¹ P ₀ ⁰	2 086 483.	(–)	–	2 086 608.	(–)	98	3s 5p	³ P ₂ ⁰	2 568 290.	(–)	–	2 567 342.	(–)

Notes. Key: *i*: level index; Conf.: configuration; Level: level IC designation; E_{th} : theoretical level energy (this work); E_{NIST} : observed energy from the NIST database (Sugar & Corliss 1985 and Shirai et al. 2000); E_{L11} : previous theoretical calculation (Landi 2011); %: percentage difference between theoretical and NIST data. All energies are in cm⁻¹.

additional factors of the excitation energy, see e.g. Bryans (2005) for specific details.

To converge the convolution integrals at high temperatures, one has to extend the calculated ordinary collision strengths to higher collision energies, it being impractical, and unnecessary, to do so explicitly using the *R*-matrix method. Instead, we calculate the infinite-energy Born and radiative dipole limits with AUTOSTRUCTURE, depending on the transition type. Once these

limits are calculated we interpolate in the Burgess–Tully scaled domain (Burgess & Tully 1992) for each specific transition type.

For Maxwellian distributions, which is the main goal of present work, we store online the effective collision strengths as a type 3 ADAS Atomic Data Format *adf04* file in the open-ADAS database. For the use of non-Maxwellian distributions it is necessary to make the original ordinary collision strengths Ω available, so that they can be convoluted by any kind of energy

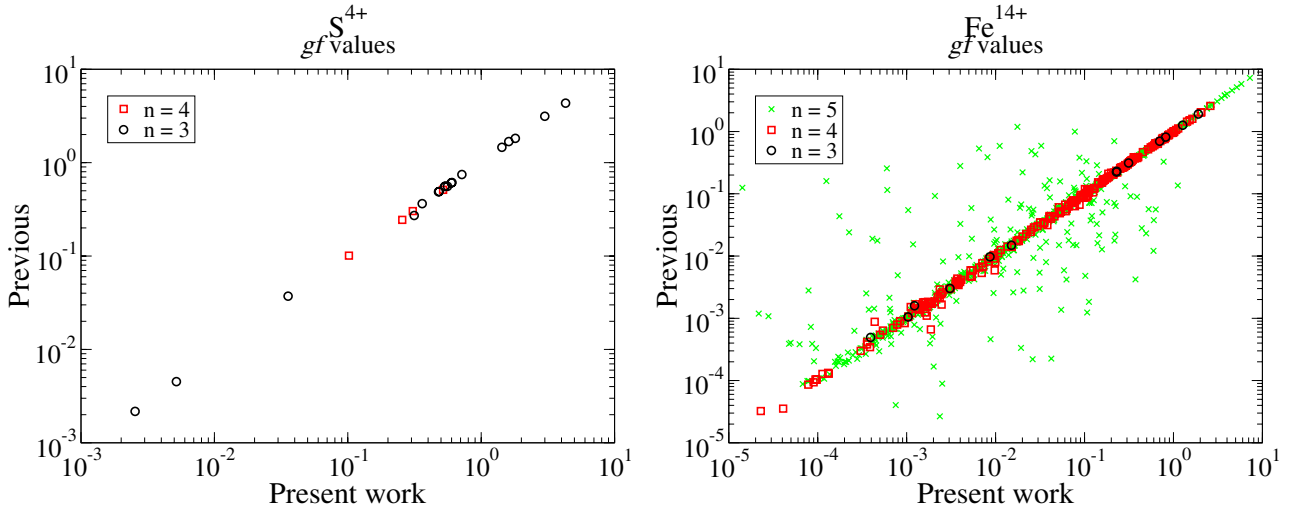


Fig. 1. Comparative plot of oscillator strengths for S^{4+} and Fe^{14+} . x axis: present work; y axis: S^{4+} (Christensen et al. 1986); Fe^{14+} (Landi 2011). These are denoted by: \circ for $n = 3$ upper levels; \square for $n = 4$ upper levels; \times for $n = 5$ upper levels.

distribution. R -matrix calculations with a few hundred levels and $\sim 10^4$ energies, such as those performed here, easily generate (compressed) Gbtye sized files. These are impractical to web-serve. To this end, we have implemented an energy-averaging of the ordinary collision strengths using a quasi-logarithmic energy mesh for the final scattered electron energy. The representation in terms of the final scattered energy maintains resolution for transitions between excited states which is lost if, as is typically done, the initial incident energy is used. The binned collision strengths (at typically 100–200 energies) are stored as a (type 5) ADAS Atomic Data Format *adf04* file, which compress to a few Mbytes.

4. Results

We calculated the ordinary collision strengths and Maxwell-averaged effective collision strengths for the electron-impact excitation of all ions in the Mg-like iso-electronic sequence, from Al^+ to Zn^{18+} , for all transitions between the 283 close-coupling fine-structure levels, which gives rise to a total of 39 903 inelastic transitions for each ion.

The effective collision strengths have been stored as a (type 3) ADAS *adf04* file. These files also contain the full set of A -values up to E3/M2 as calculated by AUTOSTRUCTURE using the structure described in Sect. 2. These data can be used for the spectroscopic diagnostic determination of the temperature and density of astrophysical and fusion plasmas.

As a sample of the results, we show in Fig. 2 the collision strengths for some important transitions within the $n = 3$ complex for the benchmark ions in the Mg-like sequence. We compare with previous distorted wave calculations of Christensen et al. (1986) for sulphur and argon, and Landi (2011) for iron. We have also performed a distorted wave calculation, using the same atomic structure as used for the R -matrix one. We show results for four different types of transitions: dipole allowed (1–5), dipole allowed through spin-orbit mixing (1–3), a double electron jump Born transition (1–7), and a forbidden one (1–10). Above the resonance region, the collision strength for dipole allowed transitions diverges logarithmically as the energy tends to infinity, while for non-dipole allowed transitions it tends to a

constant and for forbidden transitions the collision strength tends to zero as E^{-2} in the infinite energy limit.

Figure 3 shows the Maxwell-averaged effective collision strengths for the same transitions. The figure also shows a comparison with previous calculations: Christensen et al. (1986) for S^{4+} and Ar^{6+} , and Berrington et al. (2005) for Fe^{14+} .

At low temperatures the centre of the Maxwellian envelope overlies the resonance region, so at these temperatures the effective collision strength is quite sensitive to the resolution of the resonances. Thus, we have carried-out a convergence study to check that we used a fine enough electron energy mesh for the ions under consideration. The final mesh chosen was detailed in Sect. 3. The differences found with the distorted wave results of Christensen et al. (1986) and Landi (2011) at low temperatures are caused by the lack of resonance structure in the distorted wave calculations. At high temperatures, the agreement between the R -matrix and distorted waves results is quite good. The transition (1–3) shows an interesting z -dependence – spin-orbit mixing becoming increasingly important as the charge increases. For sulphur, this transition behaves as a forbidden one at temperatures of physical interest, but for iron it shows dipole-like behaviour.

The collision strengths for the Fe^{14+} 1–10 ($J = 0 - J' = 0$) transition as calculated with the R -matrix codes are up to a factor 12–18 larger than the ones obtained with the distorted wave approximation. Our distorted wave collision strengths, calculated with the same structure as with the R -matrix codes, agree with the distorted wave results of Landi (2011). They hardly change if we use instead the atomic structure of Christensen et al. (1985). So the discrepancies do not lie in the atomic structure but in the differences between the scattering methods. Looking at the same transition for the other ions shown, S^{4+} and Ar^{6+} , the differences between the results calculated with R -matrix and distorted wave remain. Note that in the plots for this transition in Fig. 2, for S^{4+} (actually, 1–13 then) and Ar^{6+} , the present distorted wave results (symbol \times) are off the bottom of the scale. The discrepancy remains and so these differences are not related to the spin-orbit interaction.

In the Burgess-Tully (Burgess & Tully 1992) reduced plots for transition 1–10 of Fe^{14+} of Fig. 4, the results of all calculations tend approximately to the same infinite energy limit point.

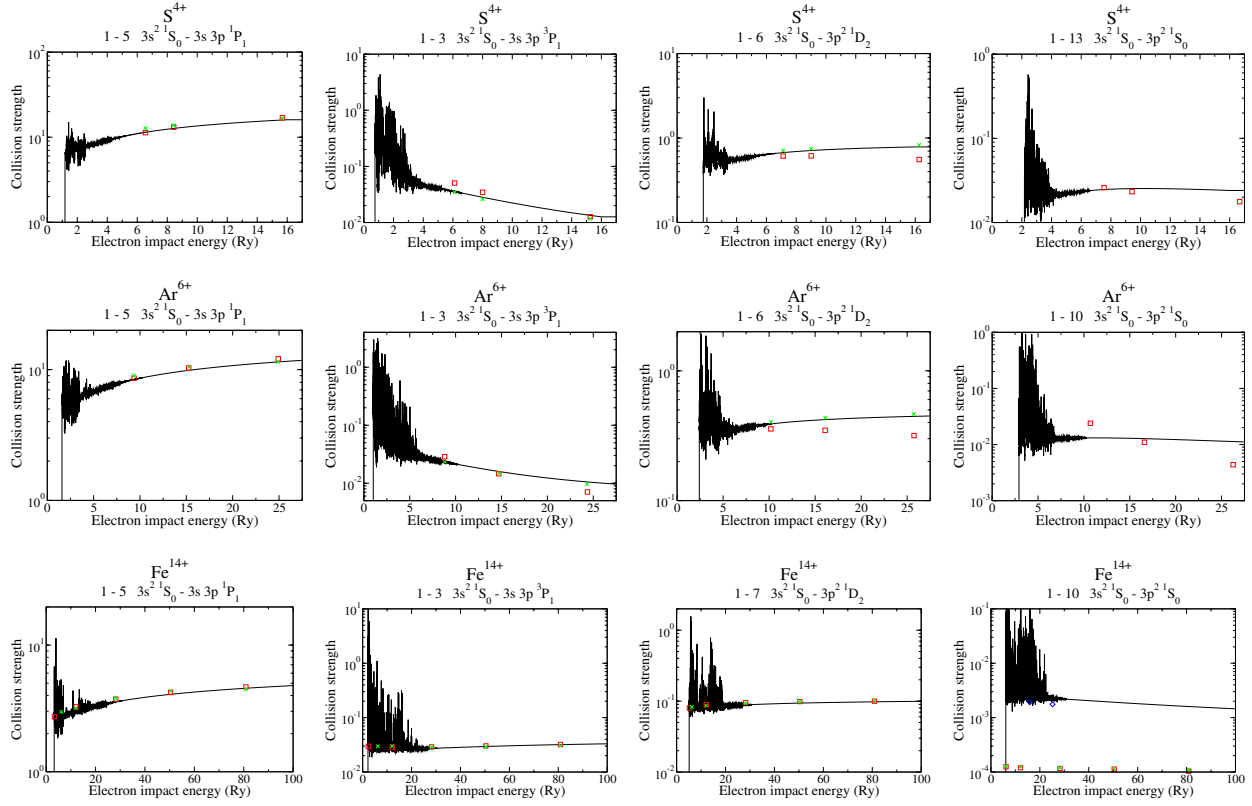


Fig. 2. Electron-impact excitation collision strengths versus the impact energy for some selected transitions within the $n = 3$ complex. Full line: present work; \times : distorted wave calculation with present structure; \square : distorted wave calculations of Christensen et al. (1986) for S^{4+} and Ar^{6+} , and Landi (2011) for Fe^{14+} ; \diamond : distorted wave calculation of Christensen et al. (1985) for Fe^{14+} .

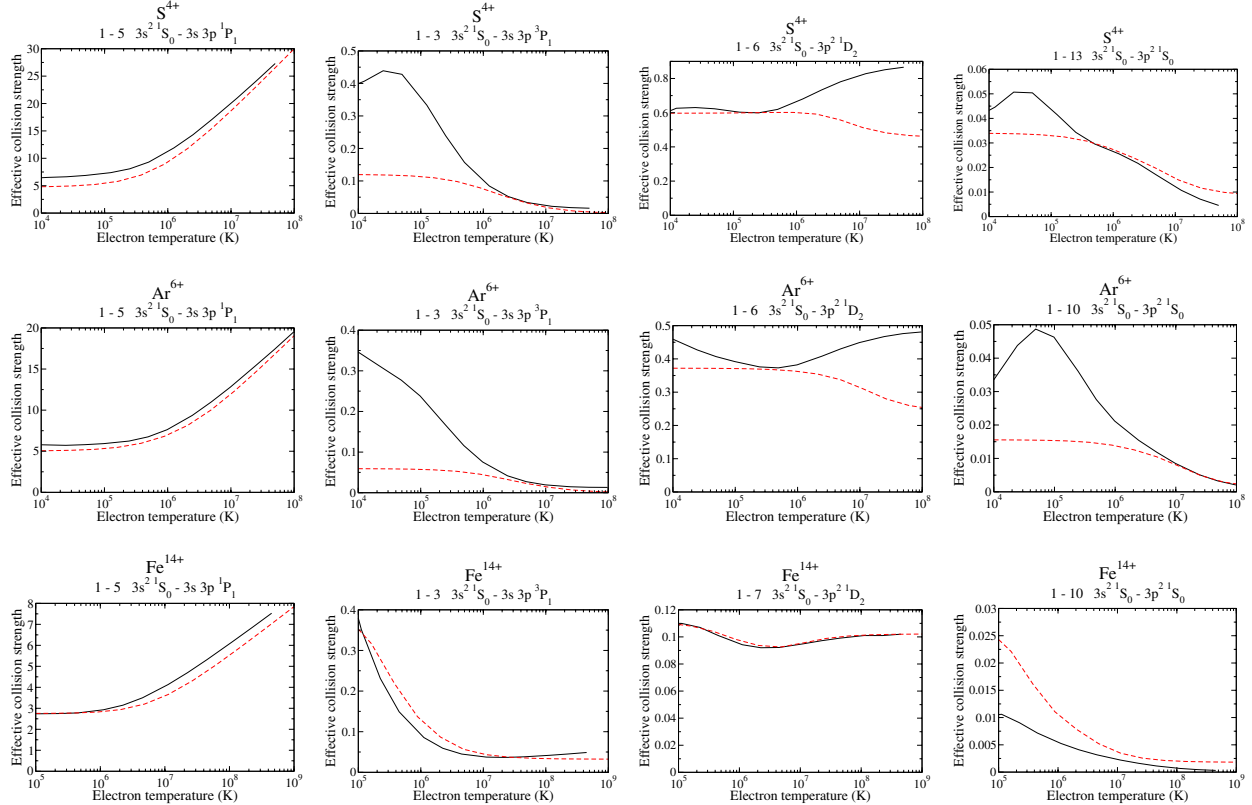


Fig. 3. Electron-impact excitation effective collision strengths versus the electron temperature for some selected transitions within the $n = 3$ complex. Full line: present calculation; dashed line: results tabulated in the CHIANTI data base, S^{4+} and Ar^{6+} Christensen et al. (1986), Fe^{14+} Berrington et al. (2005).

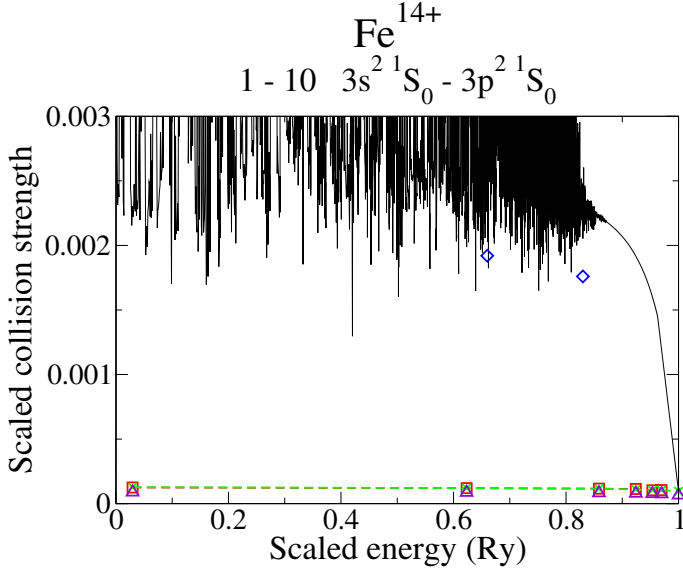


Fig. 4. Burgess-Tully scaled electron-impact excitation collision strengths for the transition 1–10: $3s^2 {}^1S_0$ – $3p^2 {}^1S_0$ in Fe^{14+} . Full line: present *R*-matrix work; \times : distorted wave calculation with the present structure; \square : distorted wave calculation of Landi (2011); \diamond : distorted wave calculation of Christensen et al. (1985); Δ : distorted wave calculations with AUTOSTRUCTURE and the atomic structure of Christensen et al. (1985).

We note that the results of Christensen et al. (1985) were calculated with the UCL-DW and JAJOM codes. These codes have the capability to convert the full K -matrix for the 16 levels to the T/S -matrices in a unitarized fashion. Both AS-DW and FAC use a two-state (initial-plus-final) conversion. The former has long been known to take account of a degree of coupling within the distorted wave formalism (e.g. Burgess et al. 1970). This is a possible explanation for the differences between the distorted wave results for this very weak transition.

The most probable decay of level 10 ($3p^2 {}^1S_0$) is the E1 transition to level 5 ($3s3p {}^1P_1^0$), with a wavelength of 325.0 Å. The 1–10 transition is a one-photon forbidden one, two electron jump, and the collision strength is small, so significant population of level 10 will come from cascading from higher levels. The CHIANTI atomic model, which uses the Berrington et al. (2005) *R*-matrix excitation data, predicts that about 64% of the population of this level is due to direct excitation from the ground state, and about 32% comes from cascading from the $3p3d {}^1P_1$ (level 26), which in turn is populated by direct excitation from the ground state by about 45%.

The intensity of the 5–10 transition is therefore partly affected by the 1–10 excitation. It is interesting to note that the CHIANTI atomic model predicts an intensity for the 5–10 325.0 Å line that is about 50% stronger than what is observed in solar active region high-resolution SERTS-97 spectra by Brosius et al. (2000). Therefore, the Berrington et al. (2005) collision strengths clearly overestimate the collision strength from the ground. Indeed our calculations predict significantly lower collision strengths than Berrington et al. (2005) for this transition (1–10, bottom right plot in Fig. 3).

As a sample of our results, we show a set of non-Maxwellian effective collision strengths for some transitions which are interesting for astrophysics. In the solar transition region the Si^{2+} ion has a maximum in the abundance fraction ($T \approx 5 \times 10^4$ K), and therefore transitions may be susceptible to non-Maxwellian

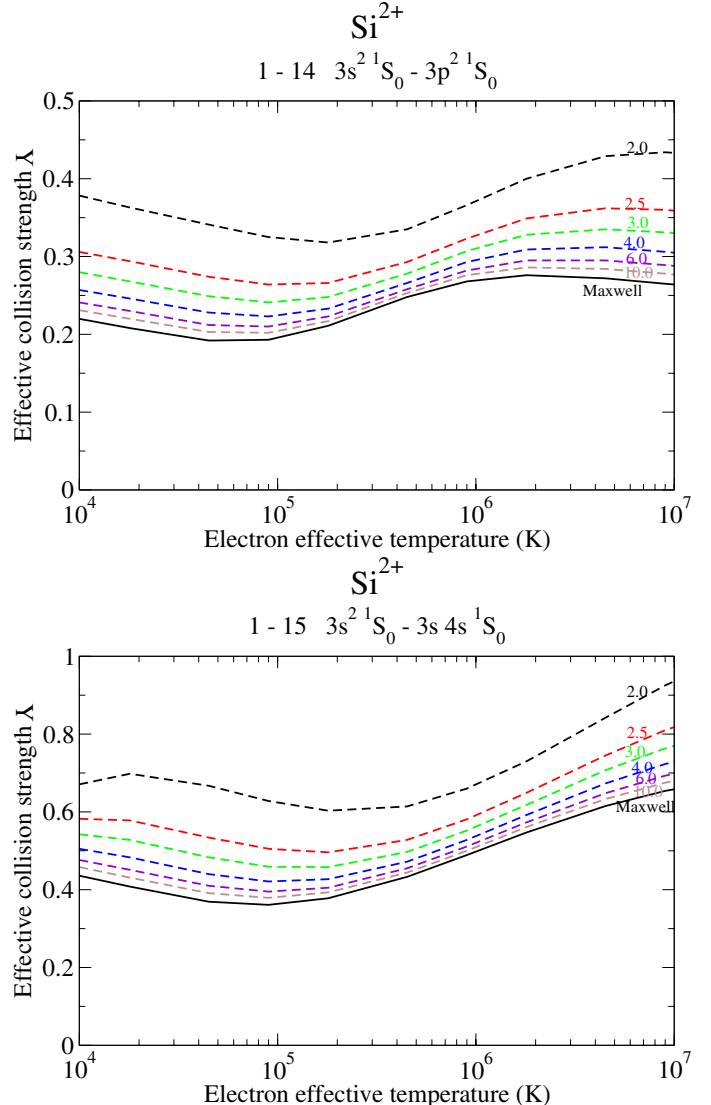


Fig. 5. Electron-impact de-excitation effective collision strengths versus effective electron temperature for selected transitions in Si^{2+} . The values of κ used for the electron velocity distribution are shown on the curves: $\kappa = 2.0, 2.5, 3.0, 4.0, 6.0, 10.0$ and ∞ in decreasing order of the effective collision strength.

distributions, for example direct excitations from the ground state to other singlets, e.g. $3p^2 {}^1D_2$, $3p^2 {}^1S_0$ or $3s4s {}^1S_0$, amongst others.

In Fig. 5 we show the effective collision strengths for Si^{2+} transitions present in solar transition region which can be affected by a non-Maxwellian distribution. These transitions are forbidden ones so their collision strengths Ω fall-off rapidly (as E^{-2}) at high collision energies. Thus, upon averaging, the effective collision strengths are sensitive to any deviation of the high energy tail of the velocity distribution from Maxwellian. This is normally represented by a κ distribution. We show results for several values of κ , converging on the Maxwellian.

5. Conclusions

We have presented a complete data set of ICFT *R*-Matrix calculations for the electron-impact excitation of all ions in the Mg-like iso-electronic sequence from Al^+ to Zn^{18+} . We have shown a selected set of collision strengths and effective collision

strengths for some important $n = 3$ transitions and ions and find good agreement with previous similar calculations, where they exist. Significant discrepancies with earlier distorted wave calculations are found. We have also presented some effective collision strengths assuming non-Maxwellian velocity distributions for the colliding electrons.

The present atomic data are a significant extension and improvement over previous ones, and are the first ones for many ions in the Mg-like sequence. With our basis set, the modelling of emission lines can now include cascading effects from levels up to $n = 5$. With the present data, emission lines from Mg-like ions can reliably be used for diagnostics of temperature and density of astrophysical and fusion plasmas.

Work is in progress to apply the same type of calculations to other iso-electronic sequences. We are carrying out calculations for the C-like, N-like and O-like sequences. Together with our previous calculations for the F-like Witthoeft et al. (2007), Ne-like Liang & Badnell (2010), Li-like Liang & Badnell (2011), Be-like Fernández-Menchero et al. (2014) and B-like Liang et al. (2009), the whole of the L-shell of iso-electronic sequences will be completed.

Acknowledgements. The present work was funded by STFC (UK) through the University of Strathclyde UK APAP network grant ST/J000892/1 and the University of Cambridge DAMTP astrophysics grant.

References

- Aggarwal, K. M. 1998, ApJSS, 118, 589
- Aggarwal, K. M., & Keenan, F. P. 1994, J. Phys. B, 27, 5321
- Badnell, N. R. 2011, Comput. Phys. Commun., 182, 1528
- Badnell, N. R., & Griffin, D. C. 2001, J. Phys. B, 34, 681
- Badnell, N. R., Griffin, D. C., & Mitnik, D. M. 2001, J. Phys. B: Atom., Mol. Opt. Phys., 34, 5071
- Berrington, K. A., Eissner, W. B., & Norrington, P. H. 1995, Comput. Phys. Commun., 92, 290
- Berrington, K. A., Ballance, C. P., Griffin, D. C., & Badnell, N. R. 2005, J. Phys. B: Atom., Mol. Opt. Phys., 38, 1667
- Bhatia, A. K., & Landi, E. 2011, At. Data Nucl. Data Tables, 97, 189
- Brosius, J. W., Thomas, R. J., Davila, J. M., & Landi, E. 2000, ApJ, 543, 1016
- Bryans, P. 2005, Ph.D. Thesis, University of Strathclyde
- Bryant, D. A. 1996, J. Plasma Phys., 56, 87
- Burgess, A. 1974, J. Phys. B: Atom. Mol. Phys., 7, L364
- Burgess, A., & Tully, J. A. 1992, A&A, 254, 436
- Burgess, A., Hummer, D. G., & Tully, J. A. 1970, Philos. Trans. R. Soc. London, Ser. A, 266, 225
- Christensen, R. B., Norcross, D. W., & Pradhan, A. K. 1985, Phys. Rev. A, 32, 93
- Christensen, R. B., Norcross, D. W., & Pradhan, A. K. 1986, Phys. Rev. A, 34, 4704
- Del Zanna, G., Fernández-Mencheno, L., & Badnell, N. R. 2014, A&A, in press, DOI: 10.1051/0004-6361/201424394
- Dere, K. P., Widing, K. G., Mason, H. E., & Bhatia, A. K. 1979, ApJSS, 40, 341
- Dudík, J., Zanna, G. D., Dzifčáková, E., Mason, H. E., & Golub, L. 2014a, ApJ, 780, L12
- Dudík, J., Zanna, G. D., Mason, H. E., & Dzifčáková, E. 2014b, A&A, 570, A124
- Dufton, P. L., & Kingston, A. E. 1989, MNRAS, 241, 209
- Dufton, P. L., Kingston, A. E., & Scott, N. S. 1983, J. Phys. B., 16, 3053
- Dufton, P. L., Kingston, A. E., & Keenan, F. P. 1984, ApJ., 280, L35
- Dzifčáková, E., & Dudík, J. 2013, ApJSS, 206, 6
- Eissner, W. 1998, Comput. Phys. Commun., 114, 295
- Eissner, W. M., Jones, M., & H. N. 1974, Comput. Phys. Commun., 8, 270
- Fernández-Mencheno, L., Zanna, G. D., & Badnell, N. R. 2014, A&A, 566, A104
- Griffin, D. C., Badnell, N. R., Pindzola, M. S., & Shaw, J. A. 1999, J. Phys. B, 32, 2139
- Gu, M. F. 2003, ApJ., 590, 1131
- Hudson, C. E., & Bell, K. L. 2006, A&A, 452, 1113
- Hudson, C. E., Norrington, P. H., & Ramsbottom, C. A. 2009, J. Phys. Conf. Ser., 163, 012060
- Hudson, C. E., Norrington, P. H., Ramsbottom, C. A., & Scott, M. P. 2012, A&A, 537, A12
- Hummer, D. G., Berrington, K. A., Eissner, W., et al. 1993, A&A, 279, 298
- Keenan, F. P., Dufton, P. L., Kingston, A. E., & Cook, J. W. 1989, ApJ, 340, 1135
- Laming, J. M., Feldman, U., Schühle, U., et al. 1997, ApJ, 485, 911
- Landi, E. 2011, At. Data Nucl. Data Tables, 97, 587
- Landi, E., Young, P. R., Dere, K. P., Zanna, G. D., & Mason, H. E. 2013, ApJ, 763, 86
- Liang, G. Y., & Badnell, N. R. 2010, A&A, 518, A64
- Liang, G. Y., & Badnell, N. R. 2011, A&A, 528, A69
- Liang, G. Y., Whiteford, A. D., & Badnell, N. R. 2009, A&A, 499, 943
- Liang, G. Y., Badnell, N. R., & Zhao, G. 2012, A&A, 547, A87
- Martin, W. C., Zalubas, R., & Musgrove, A. 1990, J. Phys. Chem. Ref. Data, 19, 821
- Martin, W. C., Sugar, J., Musgrove, A., & Dalton, G. R. 1995, NIST Database for Atomic Spectroscopy, Version 1.0, NIST Standard Reference Data base 61
- Nussbaumer, H. 1986, A&A, 155, 205
- Rubin, R. H., Dufour, R. J., & Walter, D. K. 1993, ApJ, 413, 242
- Saloman, E. B. 2010, J. Phys. Chem. Ref. Data, 39, 033101
- Saraph, H. E. 1972, A&A, 3, 256
- Shirai, T., Sugar, J., Musgrove, A., & Wiese, W. L. 2000, J. Phys. Chem. Ref. Data, Monograph N 8
- Storey, P. J., & Sochi, T. 2013, MNRAS, 430, 599
- Sugar, J., & Corliss, C. 1985, J. Phys. Chem. Ref. Data, 1
- Witthoeft, M. C., Whiteford, A. D., & Badnell, N. R. 2007, J. Phys. B: At. Mol. Opt. Phys., 40, 2969